University of Groningen

Nonlinear operator for oriented texture

Kruizinga, Peter; Petkov, Nikolay

Published in:
Ieee transactions on image processing

IMPORTANT NOTE: You are advised to consult the publisher's version (publisher's PDF) if you wish to cite from it. Please check the document version below.

Document Version
Publisher's PDF, also known as Version of record

Publication date:
1999

Nonlinear Operator for Oriented Texture

Peter Kruizinga and Nikolay Petkov

Abstract—**Texture is an important part of the visual world of animals and humans and their visual systems successfully detect, discriminate, and segment texture. Relatively recently progress was made concerning structures in the brain that are presumably responsible for texture processing. Neurophysiologists reported on the discovery of a new type of orientation selective neuron in areas V1 and V2 of the visual cortex of monkeys which they called *grating cells*. Such cells respond vigorously to a grating of bars of appropriate orientation, position and periodicity. In contrast to other orientation selective cells, grating cells respond very weakly or not at all to single bars which do not make part of a grating. Elsewhere we proposed a nonlinear model of this type of cell and demonstrated the advantages of grating cells with respect to the separation of texture and form information. In this paper, we use grating cell operators to obtain features and compare these operators in texture analysis tasks with commonly used feature extracting operators such as Gabor-energy and co-occurrence matrix operators. For a quantitative comparison of the discrimination properties of the concerned operators a new method is proposed which is based on the Fisher linear discriminant and the Fisher criterion. The operators are also qualitatively compared with respect to their ability to separate texture from form information and their suitability for texture segmentation.**

Index Terms—**Grating cells, texture analysis, texture features, visual cortex.**

I. INTRODUCTION

FEATURE-BASED classification and segmentation methods operate on a feature vector field that is the result of the application of a vector operator on an input image. Certain operators will be particularly effective for processing texture.

Several authors have made a comparison of the performance of various operators and features for texture segmentation. Most of these studies are based on the so-called classification result comparison [1]. In this method a segmentation algorithm is applied to a feature vector field and the segmentation performance and suitability of the used features are evaluated by using the number of misclassified pixels. One of the first studies based on this principle was performed by Weszka *et al.* [2]. They compared texture features based on the Fourier power spectrum, on co-occurrence matrices, and on gray level differences. Du Buf *et al.* [3] compared seven different types of texture features, including the co-occurrence matrix features as proposed by Haralick [4], the methods of Unser [5], Laws

[6], and Mitchell [7], the fractal dimension approach [8], and a method based on general operator processor (GOP) operations [9]. They used the boundary error in the segmentation result as a comparison measure. In [10] Ohanian and Dubes discussed four types of texture features, by comparing the error rates in the segmentation result. They considered co-occurrence matrix features, Gabor features [11], [12], Markov random field features [13], and fractal features. Other recent studies in which the classification result comparison method was used include [14]–[16]. The segmentation algorithms that were applied in these studies classify individual pixels using their associated feature vectors. In a recent study, Ojala *et al.* [17] used a different segmentation algorithm that performs the pixel classification on the basis of the distribution of the feature vectors in the surrounding of the concerned pixel. They compared the following four texture features: gray level differences, Laws texture features, center-symmetric covariance features, and local binary patterns. A comparison between four segmentation algorithms was made by Wang *et al.* [18] using co-occurrence matrix features. A more theoretical study was carried out by Conners and Harlow [1]. They made a comparison of the texture features that were used by Weszka *et al.* [2] and used the amount of texture-context information that is contained in the intermediate matrices as a quality measure of the texture features.

In this paper, we assess the properties of a new type of texture operator and compare it with existing texture operators. This new operator has been inspired by the function of a recently discovered type of an orientation-selective neuron in areas V1 and V2 of the visual cortex of monkeys, called the grating cell [19], [20]. About 4% of the cells in V1 and 1.6% of the cells in V2 can be characterized as grating cells and it is estimated that about 4 million grating cells in V1 subserve the central 4° of vision [20]. Similarly to other orientation selective neurons, such as simple, complex, and hyper-complex cells [21]–[23], grating cells respond vigorously to a grating of bars of appropriate orientation, position, and periodicity. In contrast to other orientation selective cells, grating cells respond very weakly or do not respond at all to single bars, this means, bars which are isolated and do not make part of a grating. This behavior of grating cells cannot be explained by linear filtering followed by half-wave rectification as in the case of simple cells [24]–[28], neither can it be explained by three-stage models of the type used for complex cells [29]–[33]. Most grating cells start to respond when a grating of a few bars (2–5) is presented. In most cases the response rises linearly with the number of bars in the grating up to a given number (4–14) after which it quickly saturates and the addition of new bars to the grating causes the response to rise only slightly or not to rise at all and in some cases

even to decline. Similarly, the response rises with the length of the bars up to a given length after which saturation and in some cases inhibition is observed. The responses to moving gratings are unmodulated and do not depend on the direction of movement. The dependence of the response on contrast shows a switching characteristic, in that turn-on and saturation contrast values lie pretty close: the most sensitive grating cells start to respond at a contrast of 1% and level off at 3%. In general, grating cells are more selective than simple cells, having half-response spatial frequency bandwidths in the range of 0.4 to 1.4 octaves, with median 1 octave, and half-response orientation bandwidths of about 20°. For comparison, simple cell spatial frequency bandwidths at half response vary in the range 0.4 to 2.6 octaves with median 1.4 octave; their median orientation bandwidth is about 40° [34].

The above properties suggest that the primary role of grating cells is to detect periodicity in oriented patterns. In previous work, we proposed a computational model of grating cells, which explains the results of the neurophysiological experiments [35], [36]. In this paper we focus on the properties of the grating cell operator as a texture analysis operator. It is compared with other, commonly used texture operators. For a quantitative comparison, however, we do not use the classification result comparison method that is used in most previous studies because this method characterizes the joint performance of a feature operator and a subsequent classifier. We rather propose a new method which characterizes the feature operator only. This method is based on a statistical approach to evaluate the capability of a feature operator to discriminate two textures by quantifying the distance between the corresponding clusters of points in the feature space according to Fisher's criterion [37], [38].

The paper is organized as follows: in Section II we review the Gabor filter; the output of the Gabor filter is used as input to the grating cell operator. Gabor-energy features that are closely related to Gabor filters are introduced. The computational model of grating cells is given in Section III. In Section IV, the co-occurrence matrix features are described. The texture analysis properties of the grating cell operator, the Gabor-energy operator, and a co-occurrence matrix based operator are examined and compared in Section V in a series of computational experiments. In Section VI we summarize the results of the study and draw conclusions.

II. Gabor Filters

Gabor filters are closely related to the function of simple cells in the primary visual cortex of primates [26], [39], [40]. Since simple cells play a substantial role in the following, we first briefly introduce a computational model of this type of cell. The response r of a simple cell which is characterized by a receptive field function $g(x, y)$ to a luminance distribution image $f(x, y)$, $(x, y) \in \Omega$, is computed as follows (Ω denotes the visual field domain):

$$r = \chi\left(\iint\limits_{\Omega} f(x, y)g(x, y)\, dx\, dy\right) \qquad (1)$$

where $\chi(z) = 0$ for $z < 0$, $\chi(z) = z$ for $z \geq 0$. Later on below we extend this simple model with local contrast normalization.

We use the following family of two-dimensional (2-D) Gabor functions [41] to model the spatial summation properties of simple cells:[1]

$$g_{\xi, \eta, \lambda, \Theta, \varphi}(x, y) = \exp\left(-\frac{x'^2 + \gamma^2 y'^2}{2\sigma^2}\right)\cos\left(2\pi\frac{x'}{\lambda} + \varphi\right)$$
$$x' = (x - \xi)\cos\Theta - (y - \eta)\sin\Theta$$
$$y' = (x - \xi)\sin\Theta + (y - \eta)\cos\Theta \qquad (2)$$

where the arguments x and y specify the position of a light impulse in the visual field and ξ, η, σ, γ, λ, Θ, and φ are parameters as follows.

The pair (ξ, η), which has the same domain Ω as the pair (x, y), specifies the *center of a receptive field* in image coordinates. The standard deviation σ of the Gaussian factor determines the (linear) *size of the receptive field*. Its eccentricity and herewith the eccentricity of the receptive field ellipse is determined by the parameter γ, called the *spatial aspect ratio*. It has been found to vary in a limited range of $0.23 < \gamma < 0.92$ [43]. The value $\gamma = 0.5$ is used in our simulations and, since this value is constant, the parameter γ is not used to index a receptive field function.

The parameter λ, which is the wavelength of the cosine factor $\cos(2\pi(x'/\lambda) + \varphi)$, determines the preferred spatial-frequency $1/\lambda$ of the receptive field function $g_{\xi, \eta, \lambda, \Theta, \varphi}(x, y)$. The ratio σ/λ determines the spatial frequency bandwidth[2] of a linear filter based on the function g.

De Valois *et al.* [34] propose that the input to higher processing stages is provided by the more narrowly tuned simple cells with half-response spatial frequency bandwidth of approximately one octave. This value of the half-response spatial frequency bandwidth corresponds to the value 0.56 of the ratio σ/λ, which is used in the simulations of this study. Since λ and σ are not independent ($\sigma/\lambda = 0.56$), only one of them is considered as a free parameter which is used to index a receptive field function. For ease of reference to the spatial frequency properties of the cells, we choose λ to be this free parameter.

The parameter Θ ($\Theta \in [0, \pi)$) specifies the *orientation* of the normal to the parallel excitatory and inhibitory stripe zones—this normal is the axis x' in (2)—which can be observed in the receptive fields of simple cells, Fig. 1(a). The value of the spatial aspect ratio and the spatial-frequency bandwidth determine the orientation bandwidth of a linear filter based on the function g. For $\gamma = 0.5$ and $b = 1.0$ octave ($\sigma/\lambda = 0.56$) the half-response orientation bandwidth of a linear filter based on g is approximately 19°.

---

[1] Our modification of the parametrization used in [41] takes into account the restrictions found in experimental data, see [42] for further details.

[2] The half-response spatial frequency bandwidth b (in octaves) of a linear filter with an impulse response according to (2) is the following function of the ratio σ/λ:

$$b = \log_2\frac{\dfrac{\sigma}{\lambda} + \dfrac{1}{\pi}\sqrt{\dfrac{\ln 2}{2}}}{\dfrac{\sigma}{\lambda} - \dfrac{1}{\pi}\sqrt{\dfrac{\ln 2}{2}}}.$$

Inversely

$$\frac{\sigma}{\lambda} = \frac{1}{\pi}\sqrt{\frac{\ln 2}{2}}\cdot\frac{2^b + 1}{2^b - 1}.$$
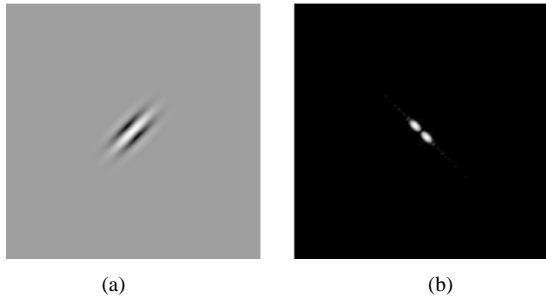
Fig. 1. Two-dimensional Gabor function in (a) space and (b) spatial frequency domain.

Fig. 2. Spatial-frequency domain coverage by the Gabor-energy filterbank used.

Finally, the parameter φ ($\varphi \in (-\pi, \pi]$), which is a phase offset in the argument of the harmonic factor $\cos(2\pi(x'/\lambda) + \varphi)$, determines the symmetry of the function $g_{\xi, \eta, \lambda, \Theta, \varphi}(x, y)$: for $\varphi = 0$ and $\varphi = \pi$ it is symmetric with respect to the center (ξ, η) of the receptive field; for $\varphi = -\frac{1}{2}\pi$ and $\varphi = \frac{1}{2}\pi$, the function is antisymmetric and all other cases are asymmetric mixtures of these two. In our simulations, we use for φ the following values: $\varphi = 0$ for symmetric receptive fields to which we refer as "center-on," $\varphi = \pi$ for symmetric receptive fields to which we refer to as "center-off," and $\varphi = -\frac{1}{2}\pi$ and $\varphi = \frac{1}{2}\pi$ for antisymmetric receptive fields with opposite polarities.

An intensity map of a receptive field function with a particular position, size, orientation, and symmetry is shown in Fig. 1(a). Fig. 1(b) shows the corresponding spatial frequency response.

Using the above parametrization, one can compute the response $s_{\xi, \eta, \lambda, \Theta, \varphi}$ of a simple cell modeled by a receptive field function $g_{\xi, \eta, \lambda, \Theta, \varphi}(x, y)$ to an input image with gray level distribution $f(x, y)$ as follows.

First, an integral

$$r_{\xi, \eta, \lambda, \Theta, \varphi} = \iint_{\Omega} f(x, y) g_{\xi, \eta, \lambda, \Theta, \varphi}(x, y) \, dx \, dy \quad (3)$$

is evaluated in the same way as if the receptive field function $g_{\xi, \eta, \lambda, \Theta, \varphi}(x, y)$ were the impulse response of a linear system. In order to normalize the simple cell response with respect to the local average luminance of the input image, $r_{\xi, \eta, \lambda, \Theta, \varphi}$ is divided by the average gray level $a_{\xi, \eta, \lambda}$ within the receptive field which is computed using the Gaussian factor of the function $g_{\xi, \eta, \lambda, \Theta, \varphi}$:

$$a_{\xi, \eta, \lambda} = \iint_{\Omega} f(x, y) \exp\left(-\frac{(x-\xi)^2 + \gamma^2(y-\eta)^2}{2\sigma^2}\right) dx \, dy. \quad (4)$$

The ratio $r_{\xi, \eta, \lambda, \Theta, \varphi}/a_{\xi, \eta, \lambda}$ is proportional to the local contrast within the receptive field of a cell modeled by the function $g_{\xi, \eta, \lambda, \Theta, \varphi}(x, y)$. In order to obtain a contrast response function similar to the ones measured on real neural cells, we use the hyperbolic ratio function to calculate the simple cell response $s_{\xi, \eta, \lambda, \Theta, \varphi}$ from the ratio $r_{\xi, \eta, \lambda, \Theta, \varphi}/a_{\xi, \eta, \lambda}$
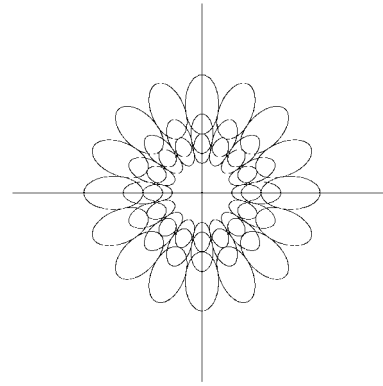
as follows:

$$s_{\xi, \eta, \lambda, \Theta, \varphi} = \begin{cases} 0, & \text{if } a = 0 \\ \chi\left(\dfrac{\dfrac{r_{\xi, \eta, \lambda, \Theta, \varphi}}{a_{\xi, \eta, \lambda}} R}{\dfrac{r_{\xi, \eta, \lambda, \Theta, \varphi}}{a_{\xi, \eta, \lambda}} + C}\right) & \text{otherwise} \end{cases} \quad (5)$$

where R and C are the maximum response level and the semisaturation constant, respectively. For further details of this model of simple cells we refer to [36].

Gabor-Energy Features: A popular set of texture features is based on the use of Gabor-filters (3) [11], [12], [44], [45] according to a multichannel filtering scheme. For this purpose, an image is filtered with a set of Gabor-filters with different preferred orientations, spatial frequencies, and phases. The filter results of the phase pairs are combined, yielding the so-called Gabor-energy quantity [11], [46], [47]:

$$E_{\xi, \eta, \Theta, \lambda} = \sqrt{r_{\xi, \eta, \Theta, \lambda, 0}^2 + r_{\xi, \eta, \Theta, \lambda, -(1/2)\pi}^2} \quad (6)$$

where $r_{\xi, \eta, \Theta, \lambda, 0}$ and $r_{\xi, \eta, \Theta, \lambda, -(1/2)\pi}$ are the outputs of the symmetric and antisymmetric filters. The Gabor-energy quantity is related to a model of complex cells which combines the responses of a quadrature phase pair of simple cells. In the experiments described in Section V, we use Gabor-energy filters with eight equidistant preferred orientations ($\Theta = 22.5°$, $\Theta = 45°$, $\cdots$, $\Theta = 180°$) and three preferred spatial frequencies ($\lambda = 5.47$, $\lambda = 8.20$, and $\lambda = 10.93$; image size $= 256$ pixels), resulting in 24-dimensional (24-D) feature vectors. The choice of three preferred spatial-frequencies and eight preferred orientations is aimed at an appropriate coverage of the spatial-frequency domain (Fig. 2). If one takes a smaller number of orientations, e.g., six instead of eight, there will be orientations to which none of the channels of the filter bank will respond sufficiently and this will have a negative effect on the discrimination performance for textures that are dominated by the concerned orientations. This means that the discrimination performance will depend on the choice of oriented texture. Similar arguments apply to the spatial-frequency discrimination. Fig. 3 illustrates the application of the filterbank on an input image which contains texture.
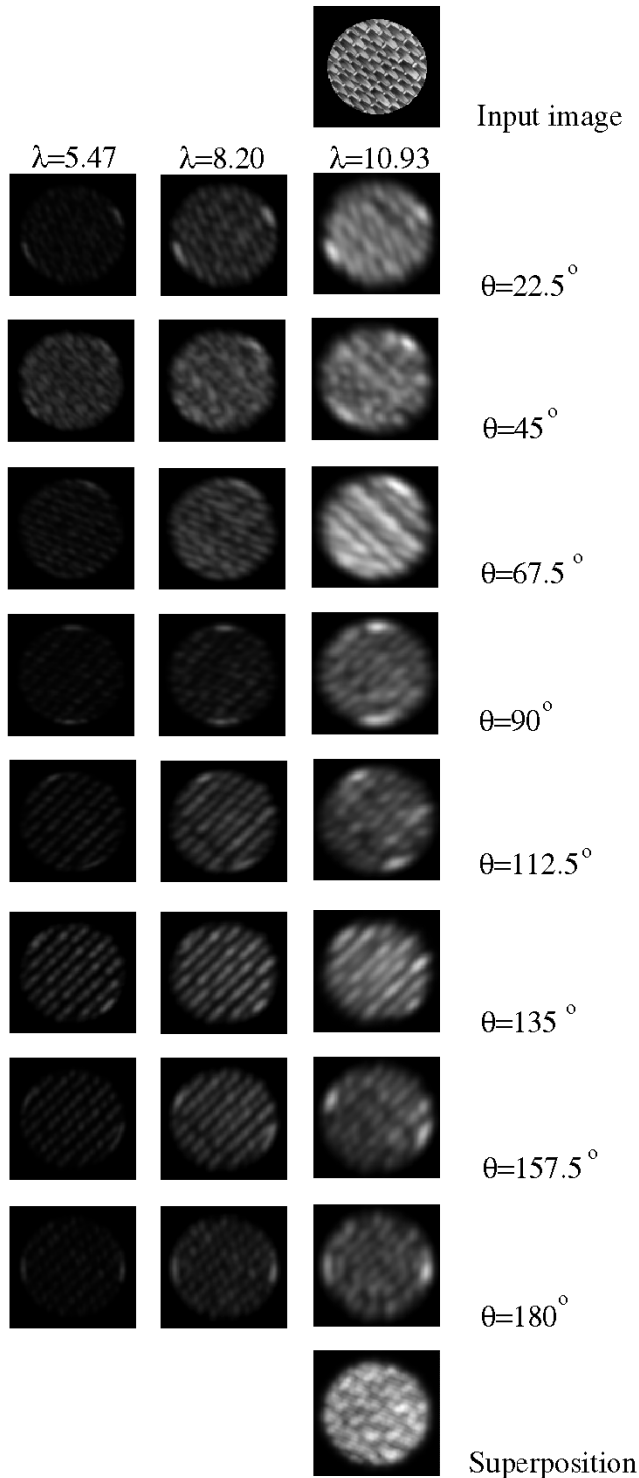
Fig. 3. Gabor-energy operator channels. The input image is shown in the top-right position. The images arranged in an 8 × 3 matrix correspond to the outputs of the different channels of the filterbank. The rows correspond to different preferred orientations, and the columns to different preferred wavelengths. The image shown in the bottom-right position is computed as a pixel-wise maximum superposition (L_∞ norm) of all channel outputs.

III. GRATING CELLS—A COMPUTATIONAL MODEL

Our model of grating cells consists of two stages [35], [36]. In the first stage, the responses of so-called *grating subunits* are computed using as input the responses of center-

on and center-off simple cells with symmetrical receptive fields. The model of a grating subunit is conceived in such a way that the unit is activated by a set of three bars with appropriate periodicity, orientation and position. In the next, second stage, the responses of grating subunits of a given preferred orientation and periodicity within a certain area are added together to compute the response of a grating cell. This model is next explained in more detail:

A quantity $q_{\xi, \eta, \Theta, \lambda}$, called the activity of a grating subunit with position (ξ, η), preferred orientation Θ and preferred grating periodicity λ, is computed as follows:

$$q_{\xi, \eta, \Theta, \lambda} = \begin{cases} 1, & \text{if } \forall n, \ M_{\xi, \eta, \Theta, \lambda, n} \geq \rho \mathcal{M}_{\xi, \eta, \Theta, \lambda} \\ 0, & \text{if } \exists n, \ M_{\xi, \eta, \Theta, \lambda, n} < \rho \mathcal{M}_{\xi, \eta, \Theta, \lambda} \end{cases} \quad (7)$$

where

$$n \in \{-3 \cdots 2\}$$

and ρ is a threshold parameter with a value smaller than but near one (e.g., $\rho = 0.9$) and the auxiliary quantities $M_{\xi, \eta, \Theta, \lambda, n}$ and $\mathcal{M}_{\xi, \eta, \Theta, \lambda}$ are computed as follows:

$$M_{\xi, \eta, \Theta, \lambda, n}$$
$$= \max \left\{ s_{\xi', \eta', \Theta, \lambda, \varphi_n} | \xi', \eta' : \right.$$
$$n \frac{\lambda}{2} \cos \Theta \leq (\xi' - \xi) < (n+1) \frac{\lambda}{2} \cos \Theta,$$
$$n \frac{\lambda}{2} \sin \Theta \leq (\eta' - \eta) < (n+1) \frac{\lambda}{2} \sin \Theta,$$
$$\varphi_n = \left. \begin{cases} 0 & n = -3, -1, 1 \\ \pi & n = -2, 0, 2 \end{cases} \right\} \quad (8)$$
$$\mathcal{M}_{\xi, \eta, \Theta, \lambda} = \max\{M_{\xi, \eta, \Theta, \lambda, n} | n = -3 \cdots 2\}. \quad (9)$$

The quantities $M_{\xi, \eta, \Theta, \lambda, n}$, $n = -3 \cdots 2$, are related to the activities of simple cells with symmetric receptive fields along a line segment of length 3λ passing through point (ξ, η) in orientation Θ. This segment is divided in intervals of length $\lambda/2$ and the maximum activity of one sort of simple cells, center-on or center-off, is determined in each interval. $M_{\xi, \eta, \Theta, \lambda, -3}$, for instance, is the maximum activity of center-on simple cells in the corresponding interval of length $\lambda/2$; $M_{\xi, \eta, \Theta, \lambda, -2}$ is the maximum activity of center-off simple cells in the adjacent interval, etc. Center-on and center-off simple cell activities are alternately used in consecutive intervals. $\mathcal{M}_{\xi, \eta, \Theta, \lambda}$ is the maximum among the above interval maxima.

Roughly speaking, the concerned grating cell subunit will be activated if center-on and center-off cells of the same preferred orientation Θ and spatial frequency $1/\lambda$ are alternately activated in intervals of length $\lambda/2$ along a line segment of length 3λ centered on point (ξ, η) and passing in direction Θ. This will, for instance, be the case if three parallel bars with spacing λ and orientation Θ of the normal to them are encountered (Fig. 4). In contrast, the condition is not fulfilled by the simple cell activity pattern caused by a single bar or two bars, only.

In the next, second stage of the model, the response $w_{\xi, \eta, \Theta, \lambda}$ of a grating cell whose receptive field is centered on point (ξ, η) and which has a preferred orientation $\Theta(\Theta \in [0, \pi))$ of the normal to the grating and periodicity
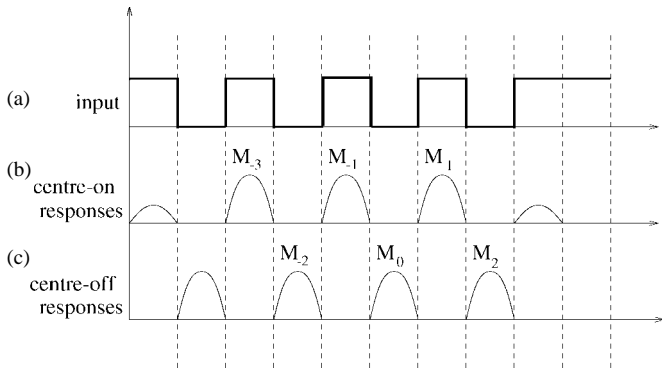
Fig. 4. Luminance distribution along a normal to a set of (a) three square bars, and the distribution of the computed responses of (b) center-on and (c) center-off cells along this line.

λ is computed by weighted summation of the responses of the grating subunits. At the same time the model is made symmetrical for opposite directions by taking the sum of grating subunits with orientations Θ and $\Theta + \pi$

$$w_{\xi, \eta, \Theta, \lambda} = \int_{\Omega} \exp\left(-\frac{(\xi - \xi')^2 + (\eta - \eta')^2}{2(\beta\sigma)^2}\right) \cdot (q_{\xi', \eta', \Theta, \lambda} + q_{\xi', \eta', \Theta+\pi, \lambda}) \, d\xi' \, d\eta',$$
$$\Theta \in [0, \pi). \tag{10}$$

The weighted summation is a provision made to model the spatial summation properties of grating cells with respect to the number of bars and their length as well as their unmodulated responses with respect to the exact position (phase) of a grating. The parameter β determines the size of the area over which effective summation takes place. A value of $\beta = 5$ results in a good approximation of the spatial summation properties of grating cells. For further details of the grating cell operator we refer to [36]. The choice of the values of model parameters ρ in (7) and in β (10) results in grating cell operators with a spatial-frequency bandwidth of about one octave and an orientation bandwidth of slightly more than $20°$, which are similar to the respective bandwidth values for the Gabor operators which provide input to the grating cell operators.

1) Grating Cell Features: The texture features proposed here, are based on the grating cell operator (7)–(10). A set of grating cell operators with eight different preferred orientations Θ and three preferred periodicities λ is applied to an image, yielding a 24-D feature vector in each image point. The same sets of values of Θ ($\Theta = 22.5°$, $\Theta = 45°$, $\cdots$, $\Theta = 180°$) and λ ($\lambda = 5.47$, $\lambda = 8.20$, and $\lambda = 10.93$) are used for the Gabor-energy and the grating cell operator filterbanks. Fig. 5 shows the results of the application of such a set of 24 grating cell operators to an input image (top-right). Note that the output is sparser than the output of the Gabor filterbank.

IV. CO-OCCURRENCE MATRIX FEATURES

A classic method for obtaining features useful for texture segmentation is based on the gray level co-occurrence matrices [4], [48], [49]. This approach is briefly reviewed in the following.
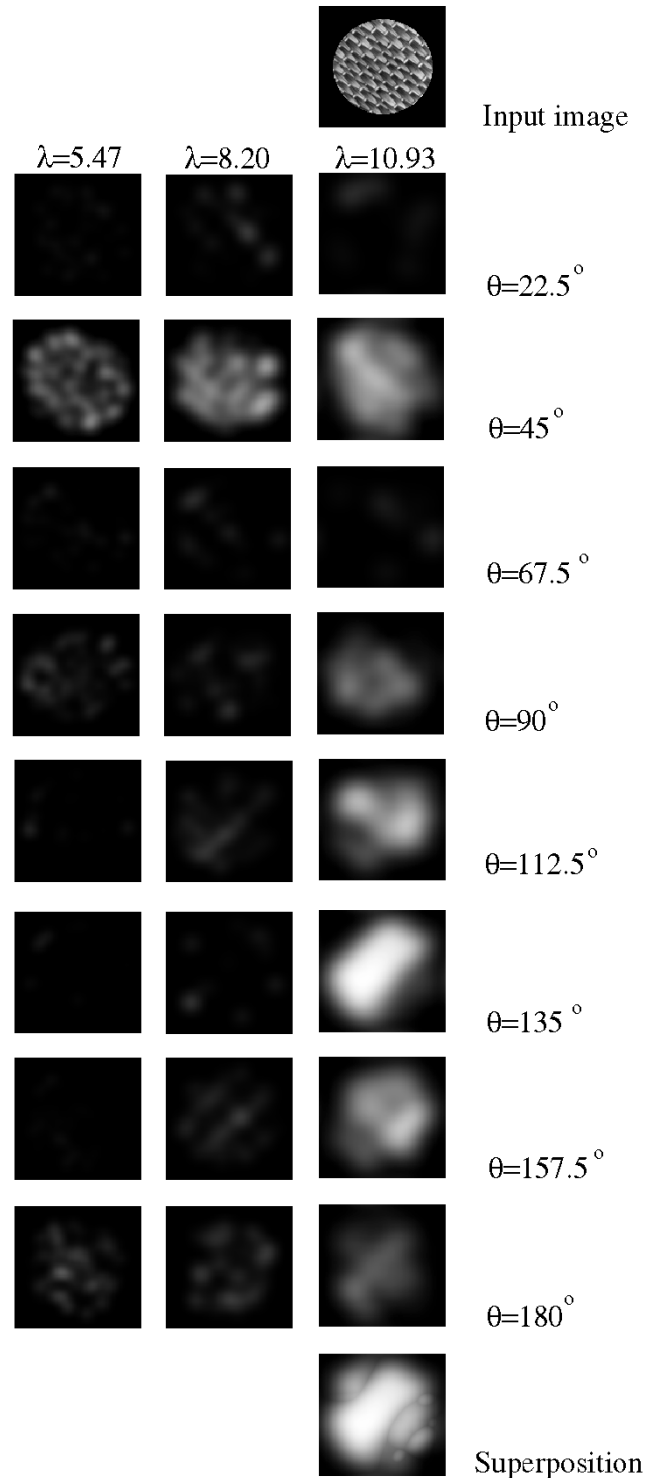
Fig. 5. Grating cell operator channels. The input image is shown in the top-right position. The images in the 8×3 matrix correspond to the outputs of the different channels of the filterbank. The rows correspond to different preferred orientations, and the columns to different preferred wavelengths. The image shown in the bottom-right position is computed as a pixel-wise maximum superposition (L_∞ norm) of all channel outputs.

In each point of a texture image, a set of gray level co-occurrence matrices is calculated for different orientations and inter-pixel distances. From these matrices features are extracted which characterize the neighborhood of the concerned pixel. The gray level co-occurrence matrix $C_{\vec{d}}(i, j)$ is defined

for a neighborhood H of a pixel, as follows:

$$C_{\vec{d}}(i, j) = \frac{1}{\text{card}(H)} \, \text{card}\Big\{\big(\vec{r}, \vec{r} + \vec{d}\big): \ \vec{r} \in H, \vec{r} + \vec{d} \in H:$$
$$I(\vec{r}) = i \wedge I\big(\vec{r} + \vec{d}\big) = j\Big\} \tag{11}$$

where $I(\vec{r})$ is the gray level in point $\vec{r}$ and i and j are gray levels. The elements of $C_{\vec{d}}$ represent the frequencies of occurrence of different gray level combinations at a distance $\vec{d}$. A large variety of texture features have been proposed by several authors, which are all based on the gray level co-occurrence matrices. In this study we use the following three features that are most commonly used:

$$\text{Energy}_{\vec{d}} = \sum_{i=0}^{G-1} \sum_{j=0}^{G-1} (C_{\vec{d}}(i, j))^2 \tag{12}$$

$$\text{Inertia}_{\vec{d}} = \sum_{i=0}^{G-1} \sum_{j=0}^{G-1} (i - j)^2 C_{\vec{d}}(i, j) \tag{13}$$

$$\text{Entropy}_{\vec{d}} = \sum_{i=0}^{G-1} \sum_{j=0}^{G-1} -C_{\vec{d}}(i, j) \log(C_{\vec{d}}(i, j)) \tag{14}$$

where G is the number of gray levels.

In our experiments we used eight vectors $\vec{d}$ (four orientations and two lengths) resulting in eight gray level co-occurrence matrices in each point. The neighborhood around each point in which the co-occurrence matrices were calculated was set to 12×12. Since three types of features (energy, inertia, and entropy) were extracted from each matrix the procedure resulted in a 24-D feature vector in each image point. Fig. 6 illustrates the effect of the application of this filter bank on an input image (top-right) which contains texture. The bottom-right image is the maximum-value superposition of all channels.

V. Texture Analysis Properties of the Operators

An often used approach to measure the performance of texture operators is to apply a segmentation algorithm to the set of feature vectors obtained by a given operator and to evaluate the segmentation performance qualitatively, based on perception, or quantitatively, based on the number of misclassified pixels. The latter method is sometimes referred to as the classification result comparison [1] and is commonly used for comparing different texture operators. In Section V-C below, we employ this qualitative method to compare the operators considered above. Before that, two further criteria are used to compare the performance of the operators.

First, the abilities of the operators to detect texture and to separate texture and form are compared, Section V-A. The general requirement for a good texture operator in this respect is that the feature vectors assigned to points, which make part of texture or in the surroundings of which there is texture, are substantially larger than the feature vectors assigned to points where there is no texture.

Second, the ability of the operators to discriminate different textures is assessed in Section V-B. The general requirements in this respect are as follows: the feature vectors assigned to
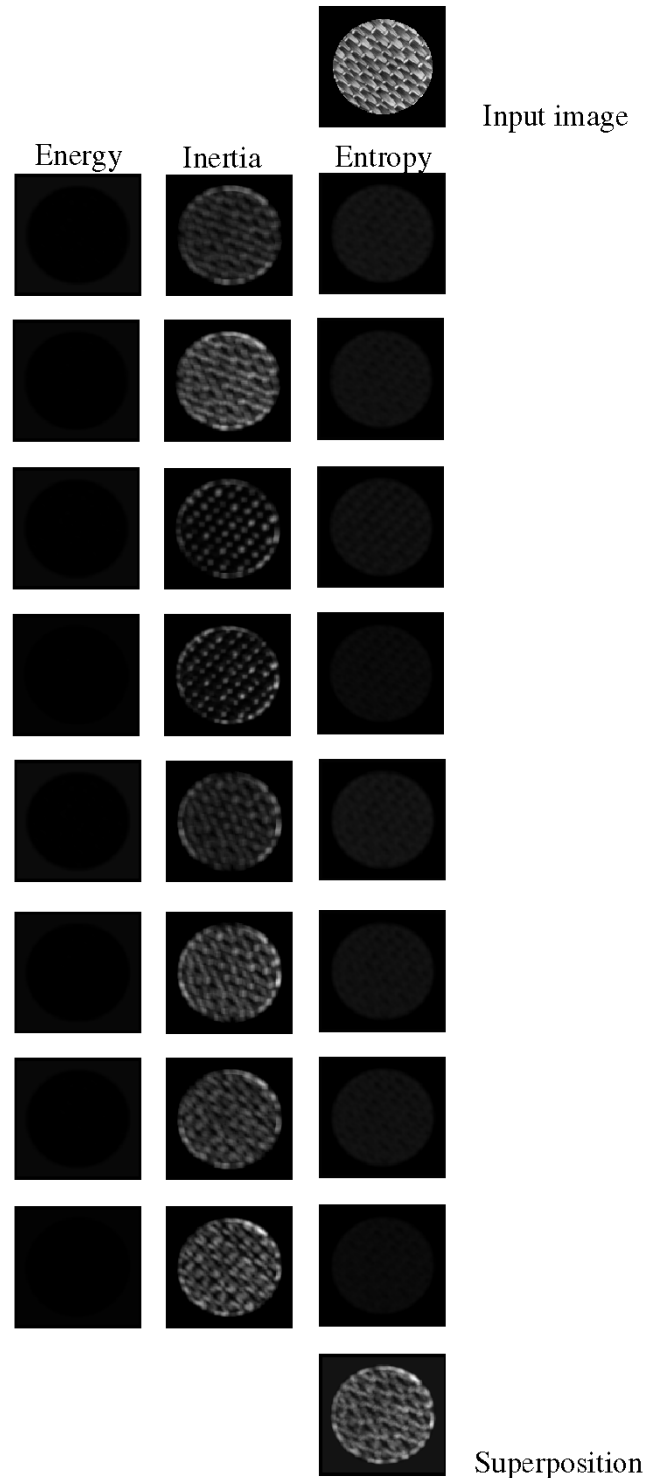
Fig. 6. Co-occurrence matrix operator channels. The three filterbank columns correspond to the co-occurrence matrix based quantities inertia, energy, and entropy. The rows correspond to different choices of the displacement vector $\vec{d}$.

the image points which lie in areas covered by the same texture should be similar (in the ideal case, they must be identical). In multivariate statistical terms, this means that these vectors form a cluster in the feature space: a contiguous region with, in comparison to the space outside the cluster, a relatively high density of feature vectors [50]. At the same time, the feature

vectors assigned to image points which belong to regions of different textures, should be different. Again in terms of clustering: the clusters of feature vectors derived from different textures should be distinct.

A. Detection of Texture and Separation of Texture and Form

We will first look at the ability of the considered operators: i) to detect texture and ii) to separate form and texture.

1) Method—Use of L_∞ Norm Features: Since the components of the vector-valued operators presented above are not isotropic and also depend on a scale parameter, no single component can be used for texture of arbitrary preferred orientation or periodicity. Therefore, we use a new scalar feature that cumulatively reflects the properties of all components of a vector operator. We choose this cumulative feature to be the length of the feature vector. For ease of computation we take the L_∞ norm according to which the length of a vector is equal to the absolute value of the largest (by absolute value) component:

$$\|\vec{x}\|_\infty = \max\{|x_1|, |x_2| \cdots |x_n|\}. \tag{15}$$

The bottom-right images in Figs. 3, 5, and 6 are computed according to (15) as a maximum-value superposition of the feature images output by the different channels of the corresponding filterbanks.

2) Results: Fig. 7 shows an input image [Fig. 7(a)] and the superposition (L_∞-norm) outputs of Gabor-energy [Fig. 7(b)], co-occurrence matrix [Fig. 7(c)], and grating cell [Fig. 7(d)] operators. All three operators give strong response in the texture area of the image and little or no response in the surrounding background of uniform gray level. We conclude that all three operators give satisfactory results for detecting oriented texture.

Fig. 8 illustrates the difference between Gabor-energy and co-occurrence matrix operators, on one hand, and grating cell operators, on the other hand, when these operators are applied to input images that contain contours but do not contain texture. In this case the co-occurrence matrix operator and the Gabor-energy operator will give misleading results, if used as texture detecting operators, because they respond not only to texture, but to other image features such as edges, lines, and contours, as well. In contrast, grating cell operators detect no features such as isolated lines and edges. In this way grating cell operators fulfill a very important requirement imposed on texture processing operators in that, next to successfully detecting (oriented) texture, they do not react to other image attributes such as object contours.

The difference between Gabor-energy and co-occurrence matrix operators, on one hand, and grating cell operators, on the other hand, is especially well illustrated when these operators are applied to images which contain both oriented texture and form information, as shown in Fig. 9. While the Gabor-energy operator [Fig. 9(b)] and the co-occurrence matrix operator [Fig. 9(c)] detect both contours and texture and are, in this way, not capable of discriminating between these two different types of image features, grating cell operators detect exclusively (oriented) texture.

(a)

(b)

(c)

(d)
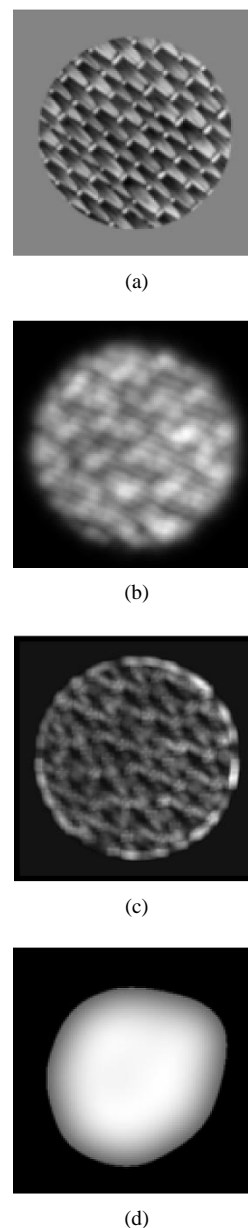
Fig. 7. Oriented texture in (a) the input image is detected by (b) Gabor energy, (c) co-occurrence matrix, and (d) grating cell operators.

We conclude that grating cell operators are more effective than Gabor-energy and co-occurrence matrix operators in the detection and processing of texture in that they are capable not only of detecting texture, but also of separating it from other image features, such as edges and contours.

B. Texture Discrimination

The clustering in the multidimensional feature space of feature vectors that originate from the same texture and the discrimination of feature vectors resulting from different textures are closely related: the compactness of a cluster of feature vectors that belong to the same texture can only be expressed in relation to the distance to other clusters.

In the following, we review a method of expressing both the intercluster distance and the compactness of the clusters in one quantity.

(a)

(b)

(c)

(d)

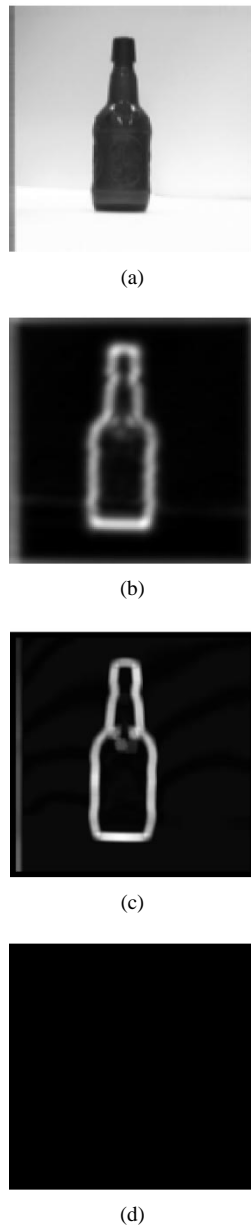Fig. 8.   While the (b) Gabor-energy operator and (c) co-occurrence matrix operator detect features, such as edges, in an input image (a) which contains no (oriented) texture, the grating cell operator (d) does not respond to nontexture image attributes.

(a)

(b)

(c)

(d)

Fig. 9.   While the (b) Gabor-energy operator and (c) the co-occurrence matrix operator detect both texture and contours in the input image (a), the grating cell operator (d) detects only texture and does not respond to other image attributes, such as contours.

1) Method—Fisher Linear Discriminant Function and Fisher Criterion: In order to determine the mutual relation between two clusters and to measure their intercluster distance, it is sufficient to look at the projection of the p-dimensional feature space (p is the number of features) onto a one-dimensional (1-D) space, under the assumption that this projection is chosen in such a way that it maximizes the separability of the clusters in the 1-D space.

The linear transformation that realizes such a projection is called *the linear discriminant function* and was first introduced by Fisher [51]. It has the following form:

$$y = (\vec{\mu}_1 - \vec{\mu}_2)^T S^{-1} \vec{x} \qquad (16)$$

where $\vec{\mu}_1$ and $\vec{\mu}_2$ are the means of the two clusters and S^{-1} is the inverse of the pooled covariance matrix.

The Fisher linear discriminant function is invariant under any nonsingular linear transformation as is easily shown. If all feature vectors $\vec{x}$ are transformed with a transformation matrix A, $\vec{x}' = A\vec{x}$, then the means of the clusters and the pooled covariance matrix are also changed: $\mu_i' = A\mu_i$ and $S' = ASA^T$. Therefore, $y' = (\vec{\mu}_1 - \vec{\mu}_2)^T A^T (ASA^T)^{-1} A\vec{x}$, so that $y' = y$.

Fig. 10 shows a sample histogram with two projected clusters with a Gaussian distribution. The separability of the two clusters is high, as can be seen from the large distance between their means η_1 and η_2 in comparison to the sum of the standard deviations σ_1 and σ_2.

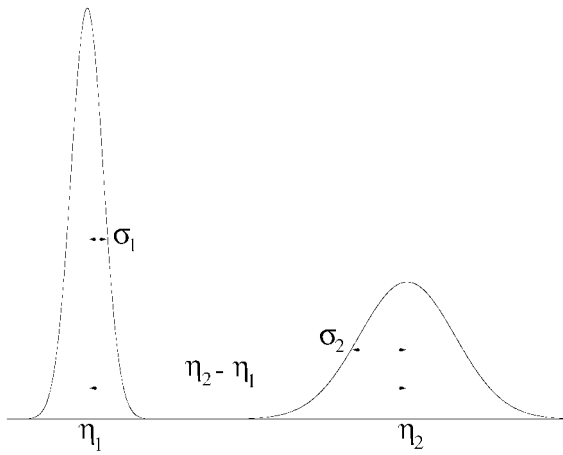Fig. 10. Two distributions of projected feature vector clusters (the horizontal axis corresponds to the position on the projection line; the vertical axis to the number of points in the image whose corresponding feature vector is projected on the same point of the projection line).

The projection of the feature vectors onto the linear discriminant maximizes the so-called Fisher criterion (see, e.g., [37] and [38]):

$$f = \frac{|\eta_1 - \eta_2|}{\sqrt{\sigma_1^2 + \sigma_2^2}} \tag{17}$$

where σ_1 and σ_2 are the variances of the distributions of the projected feature vectors of the respective clusters and η_1 and η_2 are the projected means μ_1 and μ_2 of the clusters:

$$\eta_1 = (\vec{\mu}_1 - \vec{\mu}_2)^T S^{-1} \vec{\mu}_1 \tag{18}$$
$$\eta_2 = (\vec{\mu}_1 - \vec{\mu}_2)^T S^{-1} \vec{\mu}_2. \tag{19}$$

The Fisher criterion expresses the distance between two clusters relative to their compactness in one single quantity. For this reason, the Fisher criterion is a good measure of the separability of two clusters. In contrast to the Euclidean distance metric, for example, it can be used to compare intercluster distances of clusters in different feature spaces, which enables us to qualitatively compare different texture operators. The projection of two clusters is illustrated by Fig. 11. From all possible projection lines, the Fisher linear discriminant is the one on which the Fisher criterion is maximal. Although the distance between the means of the projected feature vector distributions is larger in case of projection on Θ_2, the optimal discriminant is Θ_1, since on that line the distance between the means of the distributions is largest *relative to the sum of their variances*.

2) Results: The discrimination properties of the texture operators considered in the previous sections are now compared using a set of nine test images, each containing a single type of oriented texture (Fig. 12). For each pair of these textures, the separability is measured, using the Fisher criterion, in the following way: a 24-D vector operator of a given type is applied to the nine test textures. In this way a 24-D feature vector is assigned to each image point of the texture images. The pooled covariance matrix is calculated for each pair of textures using 1000 sample feature vectors taken from each
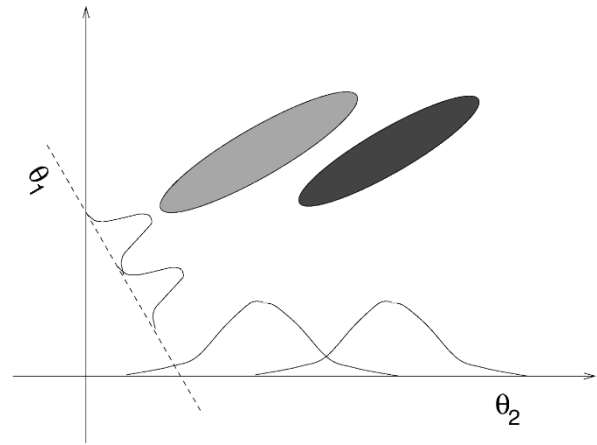
Fig. 11. In order to analyze the separability of the two clusters, the feature vectors are projected on a line. The line on which the clusters are optimally separable, in this case Θ_1, is called the Fisher linear discriminant.
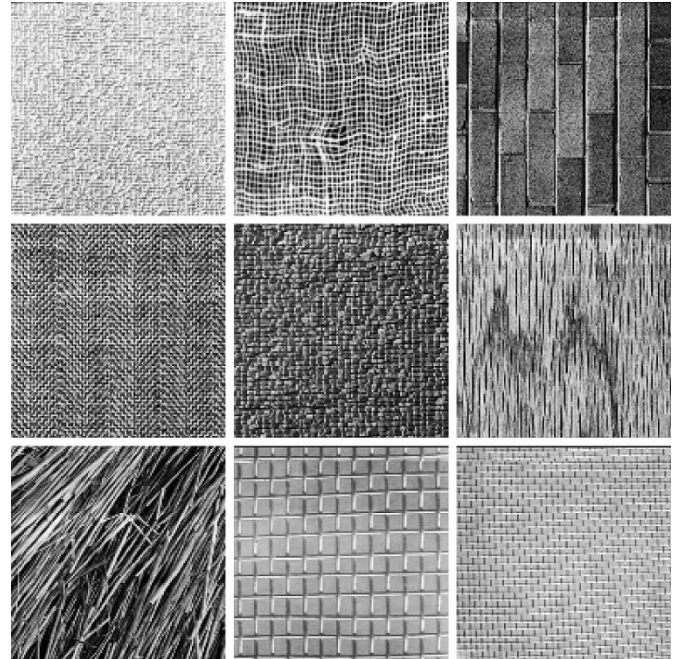
Fig. 12. Nine test images, to be denoted T1 to T9, left to right and top to bottom.

texture at random positions. Then the feature vectors are projected on a line using the Fisher linear discriminant function. In the projection space, the Fisher criterion is evaluated. Fig. 13 shows the distributions of the projected grating cell operator feature vectors of two test images (T4 and T5) along the discriminant. As can be seen from this figure, the distributions do not overlap, meaning that the clusters of feature vectors are linear separable in the feature space.

Table I shows the values of the Fisher criterion for each pair of test texture images, based on the grating cell operator features. The minimum value listed is 5.44 (for the pair of textures T3 and T7), which means that for the corresponding image pair, the projected feature vector distributions will at most overlap for no more than 0.02%. For the other texture pairs the overlap is even (much) smaller. Therefore, all clusters of feature vectors can be separated linearly. Note that the

Fig. 13. Projected versions of two clusters of feature vectors derived from different textures. Since the distributions of projected feature vectors do not overlap, the original clusters of feature vectors are linearly separable.

TABLE I
VALUES OF THE FISHER CRITERION f
OBTAINED WITH THE GRATING CELL OPERATOR

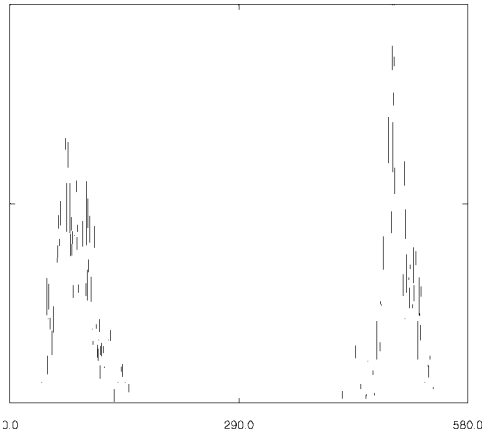|	T1	T2	T3	T4	T5	T6	T7	T8	T9
T1	-	6.24	13.53	13.05	6.57	11.65	14.19	17.56	19.09
T2		-	10.75	9.12	6.86	8.03	8.74	14.89	12.77
T3			-	20.77	13.85	8.72	5.44	9.55	26.22
T4				-	11.06	22.39	14.52	27.36	31.62
T5					-	11.24	13.52	18.13	14.53
T6						-	6.52	8.69	15.66
T7							-	8.82	21.04
T8								-	22.13
T9									-

TABLE II
VALUES OF THE FISHER CRITERION FISHER CRITERION
OBTAINED WITH THE GABOR-ENERGY OPERATOR

	T1	T2	T3	T4	T5	T6	T7	T8	T9
T1	-	5.84	6.97	8.10	4.99	6.81	7.22	6.05	8.65
T2		-	4.31	6.42	3.77	4.36	4.25	4.39	7.70
T3			-	8.67	4.83	2.35	4.32	4.52	8.28
T4				-	7.33	9.32	7.07	9.75	12.89
T5					-	4.58	4.42	4.93	7.18
T6						-	4.11	3.60	8.67
T7							-	4.47	9.40
T8								-	7.26
T9									-

TABLE III
VALUES OF THE FISHER CRITERION OBTAINED
WITH THE CO-OCCURRENCE MATRIX OPERATOR

	T1	T2	T3	T4	T5	T6	T7	T8	T9
T1	-	4.76	4.78	4.48	4.15	4.68	4.51	5.26	5.08
T2		-	3.35	4.26	3.15	4.61	3.94	4.59	4.19
T3			-	4.77	3.16	3.49	3.56	4.29	4.63
T4				-	4.35	5.20	4.45	5.62	5.58
T5					-	4.19	3.55	4.57	4.36
T6						-	3.54	4.30	5.54
T7							-	4.26	4.95
T8								-	3.17
T9									-

feature vectors of a cluster are taken from an image that contains merely one texture. This means that it is *a priori* known to which cluster the feature vector samples belong to, resulting in a good estimate of the covariance matrix.

The values of the Fisher criterion obtained with the grating cell operator for any pair of the used test images are so high that a linear separation of the clusters is always possible. Therefore the conclusion is justified that the grating cell operator has excellent discrimination properties.

Table II shows the values of the Fisher criterion for pairs of clusters of feature vectors, derived from the nine different textures, using the Gabor-energy texture features. The values listed in Table II are all smaller than the corresponding values obtained with the grating cell operator (Table I). On average, the Fisher criterion for the Gabor-energy features is more than two times smaller than the one for the grating cell operator. However, the Fisher criterion is still sufficiently large so that the clusters are distinguishable. The Gabor-energy features are therefore also suitable for oriented texture discrimination. For the segmentation of a texture image into regions containing the same texture, i.e., for the classification of individual pixels, the intercluster distance is not sufficient.

The Fisher criterion was also calculated using the co-occurrence matrix features. The results are shown in Table III. The average intercluster distance is even smaller than in the case of the Gabor-energy features. On average it is three times smaller compared to the values obtained with the grating cell operator features. The intercluster distances are, however, still large enough to separate the clusters as a whole.

The conclusion which can be drawn from these experiments is that the grating cell operator shows the best discrimination properties, at least as far as oriented textures are concerned.

C. Automatic Texture Segmentation

We carried out a number of texture segmentation experiments in which a general purpose clustering algorithm was applied to the feature vectors obtained with the operators discussed above.

1) Method—Segmentation Using the K-Means Clustering Algorithm: The K-means clustering algorithm [52] was used for segmentation. It is based on the following cluster criterion:

$$\vec{x} \in A \quad \text{if } \forall (B: B \neq A: d(\vec{x}, \vec{\mu}_A) < d(\vec{x}, \vec{\mu}_B)) \qquad (20)$$

where A and B are clusters, $\vec{\mu}_A$ and $\vec{\mu}_B$ are the respective mean feature vectors, and $d(\vec{x}, \vec{y})$ is the distance between two feature vectors $\vec{x}$ and $\vec{y}$. In our experiments we used the Euclidean distance. The K-means clustering procedure is as follows:

1) Initially, K cluster mean vectors are chosen randomly.
2) Next, all feature vectors are assigned to one of the K clusters using the above criterion.
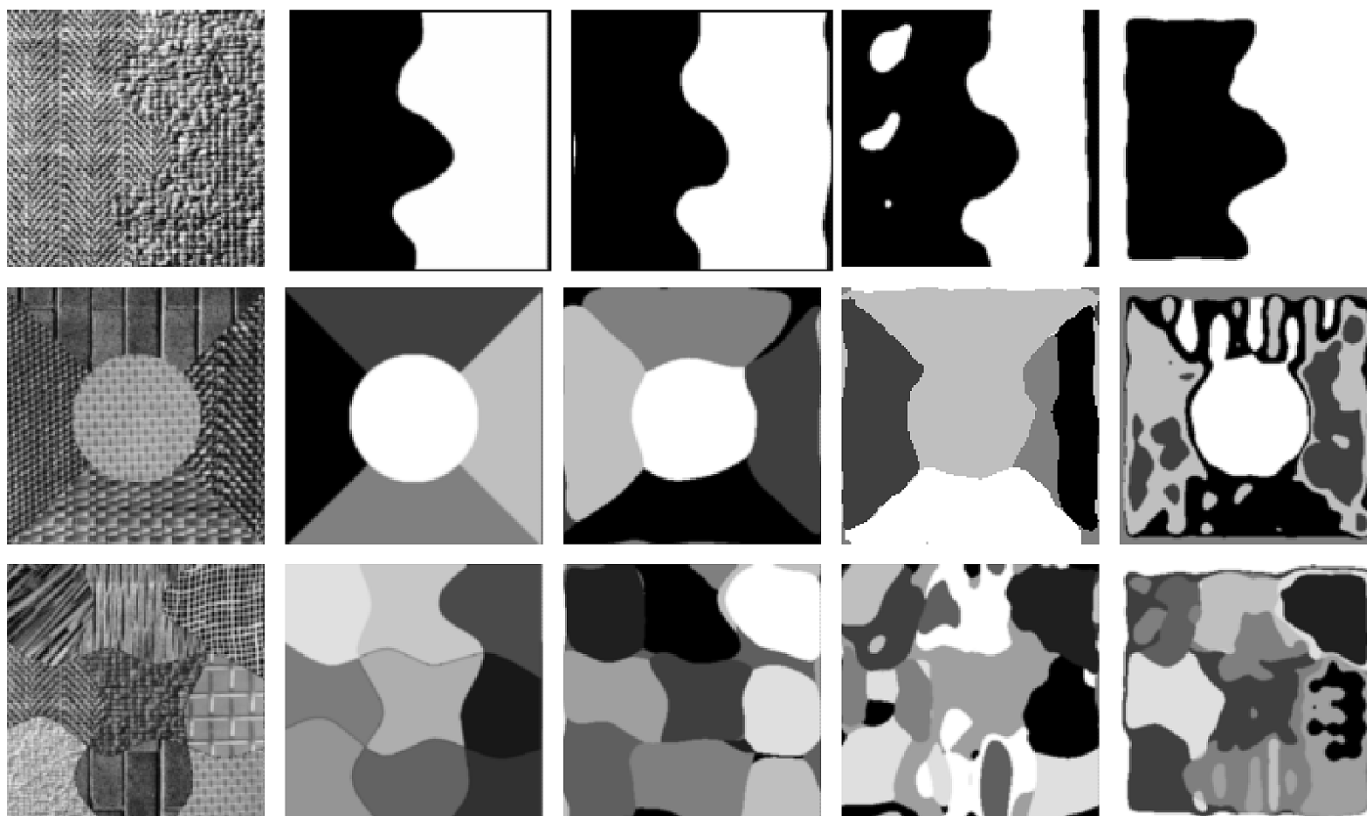
Fig. 14. Results of segmentation experiments using the K-means clustering algorithm. The left-most column shows three input images containing two, five, and nine textures. The second column shows the exact segmentation of the input images (i.e., the so-called ground truth). The three right-most columns show the segmentation results (using $K = 2$, $K = 5$, and $K = 9$ for the respective rows) based on the grating cell operator (middle column), the Gabor-energy operator (second column from the right), and the co-occurrence matrix operator (right-most column).

3) Each cluster mean is updated by computing it as the mean of all feature vectors that were assigned to the concerned cluster.

4) Steps 2 and 3 are repeated until a certain convergence criterion is fulfilled.

2) Results: In order to compare the texture segmentation performance of the grating cell operator with the two other texture operators, we applied the operators to three test images to obtain feature vector fields to which the K-means segmentation algorithm was applied. The results are shown in Fig. 14. The leftmost column shows the input images with two, five, and nine different textures, respectively. The perfect segmentations (ground truth) of these images are shown in the second column. The other three columns show the segmentation results based on the three vector operators considered above.

It is clear that the results obtained with the grating cell features are considerably better than the results obtained with the other two types of features. The only misclassified pixels are located near the texture borders. This is due to the fact that two or more different textures fall in the receptive field of the grating cell operator, causing an inaccurate estimate of the feature vector. Because of the large distance between the clusters of feature vectors, such inaccurate estimates do not immediately result in misclassification.

The segmentation based on the Gabor-energy operator features (Fig. 14, second column from the right) is clearly worse than the one based on the grating cell operator. Even the segmentation of two textures is poor. When more different textures are added, segmentation performance decreases rapidly. Pixels are classified incorrectly not only at the texture border but also inside a texture region. The rightmost column of Fig. 14 shows the segmentation results obtained with the co-occurrence matrix operator. The same effect is observed as with the Gabor-energy operator. The segmentation of the image which contains just two texture images is correct, but for more than two textures, the segmentation results get worse very quickly.

VI. SUMMARY AND CONCLUSIONS

In this paper, we compared two well-known texture operators, the co-occurrence matrix operator and the Gabor-energy operator, with a new biologically motivated nonlinear texture operator, the *grating cell operator,* which was proposed elsewhere by the authors.

First, we evaluated the ability of the operators to detect texture and to separate texture and form information. By applying the operators to an image that does not contain texture and an image that contains both texture and form, we showed that the co-occurrence matrix operator and the

Gabor-energy operator fail to distinguish between form and texture information. The energy feature channels of the co-occurrence matrix operator respond to regions of uniform gray level and both the co-occurrence matrix operator and the Gabor-energy operator respond to contours and edges. In contrast, the grating cell operator responds to oriented texture only. Elsewhere, we proposed a complementary operator that responds only to contours and edges, but does not respond to texture [36].

Second, we studied the discrimination properties of the concerned texture operators using a new quantitative comparison method based on the Fisher criterion. We investigated whether the feature vectors extracted from a single texture form a cluster in the feature space and whether feature vector clusters that originate from different textures can be distinguished. The Fisher linear discriminant function was applied to project the feature vectors on a 1-D feature space (line). The distance between the projected cluster means, relative to the sum of the variances of the projected cluster distributions, which is called the Fisher criterion, was used as a measure of the separability of the feature vector clusters. This method was applied to measure the intercluster distances for each pair of nine images containing oriented texture. On average the relative distance between the feature vector clusters obtained with the grating cell operator was twice as large as the relative distance between the clusters obtained with the Gabor-energy operator and about three times as large as the distance between the clusters resulting from the co-occurrence matrix operator.

Third, a number of texture segmentation experiments was performed in which a general purpose clustering algorithm was employed to cluster the feature vectors within the feature vector fields resulting from the application of the three concerned texture operators. The standard K-means algorithm was used to cluster the feature vectors which were extracted from an input image containing two or more different textures. The outcome of the experiments confirmed the superiority of the grating cell operator, especially when a larger number of textures was to be segmented.

A final remark is due on the purpose of this study. Our aim was not to propose just another texture operator and to demonstrate its advantages in comparison to (a limited number of) other texture operators when applied to certain image material. The main purpose was to present to the image processing and computer vision research community a texture operator that closely models the texture processing properties of the visual system of monkeys and, most probably, of humans. In this respect, the grating cell operator cannot be considered as just another texture operator. The comparison with other operators was not done in order to prove superiority (or inferiority). This comparison was done, rather, to satisfy our curiosity (and, hopefully, the curiosity of other researchers) about how an operator that is employed by natural vision systems performs in comparison to artificial operators that are devised by man. Neither was image material selected in order to prove a specific point. The image material was arbitrarily chosen with the only restrictions being that the concerned textures be oriented and look natural. The first restriction is justified by the proposed biological role of grating cells and

by the insights in its function. The second one is due to the understanding that natural vision mechanisms are optimally fitted to a natural environment. In this context and under the mentioned restrictions, the results of the study can be considered satisfactory.

REFERENCES

[1] R. W. Conners and C. A. Harlow, "A theoretical comparison of texture algorithms," *IEEE Trans. Pattern Anal. Machine Intell.,* vol. PAMI-2, pp. 204–222, 1980.

[2] J. S. Weszka, C. R. Dyer, and A. Rosenfeld, "A comparative study of texture measures for terrain classification," *IEEE Trans. Syst., Man, Cybern.,* vol. SMC-6, pp. 269–285, 1976.

[3] J. M. H. Du Buf, M. Kardan, and M. Spann, "Texture feature performance for image segmentation," *Pattern Recognit.,* vol. 23, pp. 291–309, 1990.

[4] R. M. Haralick, K. Shanmugam, and I. Dinstein, "Textural features for image classification," *IEEE Trans. Syst., Man, Cybern.,* vol. SMC-3, pp. 610–621, 1973.

[5] M. Unser, "Local linear transforms for texture measurements," *Signal Process.,* vol. 11, pp. 61–79, 1986.

[6] K. I. Laws, "Textured image segmentation," Tech. Rep. USCIPI 940, Image Process. Inst., Univ. South. Calif., 1980.

[7] O. R. Mitchell, C. R. Myers, and W. Boyne, "A max–min measure for image texture analysis," *IEEE Trans. Comput.,* vol. C-2, pp. 408–414, 1977.

[8] S. Peleg, J. Naor, R. Hartley, and D. Avnir, "Multiple resolution texture analysis and classification," *IEEE Trans. Pattern Anal. Machine Intell.,* vol. PAMI-6, pp. 514–523, 1984.

[9] H. Knutsson and G. H. Granlund, "Texture analysis using two-dimensional quadrature filters," in *Proc. IEEE Workshop CAPAIDM,* Pasadena, CA, 1983.

[10] P. P. Ohanian and R. C. Dubes, "Performance evaluation for four classes of textural features," *Pattern Recognit.,* vol. 25, pp. 819–833, 1992.

[11] M. R. Turner, "Texture discrimination by Gabor functions," *Biol. Cybern.,* vol. 55, pp. 71–82, 1986.

[12] I. Fogel and D. Sagi, "Gabor filters as texture discriminator," *Biol. Cybern.,* vol. 61, pp. 103–113, 1989.

[13] G. R. Cross and A. K. Jain, "Markov random field texture models," *IEEE Trans. Pattern Anal. Machine Intell.,* vol. PAMI-I5, pp. 25–39, 1983.

[14] Y. M. Zhu and R. Goutte, "A comparison of bilinear space spatial-frequency representations for texture discrimination," *Pattern Recognit. Lett.,* vol. 16, pp. 1057–1068, 1995.

[15] O. Pichler, A. Teuner, and B. J. Hosticka, "A comparison of texture feature extraction using adaptive gabor filtering, pyramidal and tree structured wavelet transforms," *Pattern Recognit.,* vol. 29, pp. 733–742, 1996.

[16] K. V. Ramana and B. Ramamoorthy, "Statistical methods to compare the texture features of machined surfaces," *Pattern Recognit.,* vol. 29, pp. 1447–1460, 1996.

[17] T. Ojala, M. Pietikainen, and D. Harwood, "A comparative study of texture measures with classification based on feature distributions," *Pattern Recognit.,* vol. 29, pp. 51–59, 1996.

[18] Z. L. Wang, A. Guerriero, and M. Desario, "Comparison of several approaches for the segmentation of texture images," *Pattern Recognit. Lett.,* vol. 17, pp. 509–521, 1996.

[19] R. von der Heydt, E. Peterhans, and M. R. Dürsteler, "Grating cells in monkey visual cortex: Coding texture?," in *Channels in the Visual Nervous System: Neurophysiology, Psychophysics and Models,* B. Blum, Ed.   London, U.K.: Freund, 1991, pp. 53–73.

[20] ———, "Periodic-pattern-selective cells in monkey visual cortex," *J. Neuroscience,* vol. 12, pp. 1416–1434, 1992.

[21] D. H. Hubel and T. N. Wiesel, "Receptive fields, binocular interaction and functional architecture in the cat's visual cortex," *J. Physiol.,* vol. 160, pp. 106–154, 1962.

[22] ———, "Sequence regularity and geometry of orientation columns in the monkey striate cortex," *J. Comput. Neurol.,* vol. 158, pp. 267–293, 1974.

[23] D. H. Hubel, "Exploration of the primary visual cortex, 1955–78," *Nature,* vol. 299, pp. 515–524, 1982.

[24] B. W. Andrews and D. A. Pollen, "Relationship between spatial frequency selectivity and receptive field profile of simple cells," *J. Physiol.,* vol. 287, pp. 163–176, 1979.

[25] V. D. Glezer, T. A. Tsherbach, V. E. Gauselman, and V. M. Bondarko, "Linear and nonlinear properties of simple and complex receptive fields in area 17 of the cat visual cortex," *Biol. Cybern.,* vol. 37, pp. 195–208, 1980.

[26] J. J. Kulikowski and P. O. Bishop, "Fourier analysis and spatial representation in the visual cortex," *Experientia,* vol. 37, pp. 160–163, 1981.

[27] L. Maffei, M. C. Morrone, M. Pirchio, and G. Sandini, "Responses of visual cortical cells to periodic and nonperiodic stimuli," *J. Physiol.,* vol. 296, pp. 27–47, 1979.

[28] J. A. Movshon, I. D. Thompson, and D. J. Tolhurst, "Spatial summation in the receptive fields of simple cells in the cat's striate cortex," *J. Physiol.,* vol. 283, pp. 53–77, 1978.

[29] M. C. Morrone and D. C. Burr, "Feature detection in human vision: Aphase-dependent energy model," in *Proc. R. Soc. Lond. B,* vol. 235, pp. 221–245, 1988.

[30] J. A. Movshon, I. D. Thompson, and D. J. Tolhurst, "Receptive field organization of complex cells in the cat's striate cortex," *J. Physiol.,* vol. 283, pp. 79–99, 1978.

[31] R. Shapley, T. Caelli, M. Morgan, and I. Rentschler, "Computational theories of visual perception," in *Visual Perception: The Neurophysiological Foundations,* L. Spillmann and J. S. Werner, Eds. New York: Academic, 1990, pp. 417–448.

[32] H. Spitzer and S. Hochstein, "A complex-cell receptive-field model," *J. Neurosci.,* vol. 53, pp. 1266–1286, 1985.

[33] R. G. Szulborski and L. A. Palmer, "The two-dimensional spatial structure of nonlinear subunits in the receptive fields of complex cells," *Vis. Res.,* vol. 30, pp. 249–254, 1990.

[34] R. L. DeValois, D. G. Albrecht, and L. G. Thorell, "Spatial frequency selectivity of cells in macaque visual cortex," *Vis. Res.,* vol. 22, pp. 545–559, 1982.

[35] P. Kruizinga and N. Petkov, "A computational model of periodic-pattern-selective cells," in *Proc. IWANN'95,* Lecture Notes in Computer Science vol. 930, J. Mira and F. Sandoval, Eds. Berlin, Germany: Springer-Verlag, 1995, pp. 90–99.

[36] N. Petkov and P. Kruizinga, "Computational models of visual neurons specialised in the detection of periodic and aperiodic oriented visual stimuli: Bar and grating cells," *Biol. Cybern.,* vol. 76, pp. 83–96, 1997.

[37] K. Fukunaga, *Introduction to Statistical Pattern Recognition.* New York: Academic, 1990.

[38] R. J. Schalkoff, *Pattern Recognition: Statistical, Structural and Neural Approaches.* New York: Wiley, 1992.

[39] J. G. Daugman, "Two-dimensional spectral analysis of cortical receptive field profiles," *Vis. Res.,* vol. 20, pp. 847–856, 1980.

[40] S. Marčelja, "Mathematical description of the response of simple cortical cells," *J. Opt. Soc. Amer.,* vol. 70, pp. 1297–1300, 1980.

[41] J. G. Daugman, "Uncertainty relation for resolution in space, spatial frequency, and orientation optimized by two-dimensional visual cortical filters," *J. Opt. Soc. Amer. A,* vol. 2, pp. 1160–1169, 1985.

[42] N. Petkov, "Biologically motivated computationally intensive approaches to image pattern recognition," *Future Generation Comput. Syst.,* vol. 11, pp. 451–465, 1995.

[43] J. P. Jones and A. Palmer, "An evaluation of the two-dimensional Gabor filter model of simple receptive fields in cat striate cortex," *J. Neurophys.,* vol. 58, pp. 1233–1258, 1987.

[44] A. K. Jain and F. Farrokhnia, "Unsupervised texture segmentation using Gabor filters," *Pattern Recognit.,* vol. 24, pp. 1167–1186, 1991.

[45] S. Y. Lu, J. E. Hernandez, and G. A. Clar, "Texture segmentation by clustering of Gabor feature vector," in *Proc. Int. Joint Conf. Neural Networks,* 1991, pp. 683–688.

[46] J. R. Bergen and M. S. Landy, "Computational modeling of visual texture segregation," in *Computational Models of Visual Processing,* M. S. Landy and J. A. Movshon, Eds. Cambridge, MA: MIT Press, 1991, ch. 17, pp. 253–271.

[47] T. N. Tan, "Texture edge detection by modeling visual cortical channels," *Pattern Recognit.,* vol. 28, pp. 1283–1298, 1995.

[48] A. Visa, "Texture classification and segmentation based on neural network methods," Ph.D. dissertation, Helsinki Univ. Technol., Finland, 1990.

[49] S. H. Peckingpaugh, "An improved method for computing gray-level co-occurrence matrix based texture measures," *Comput. Vis., Graph., Image Process.: Graph. Models and Image Process.,* vol. 53, pp. 574–580, 1991.

[50] B. Everitt, *Cluster Analysis.* London, U.K.: Heinemann Educational Books, 1974.

[51] A. Fisher, *The Mathematical Theory of Probabilities.* New York: Macmillan, 1923, vol. 1.

[52] J. MacQueen, "Some methods for classification and analysis of multivariate observations," in *Proc. 5th Berkeley Symp. Mathematical Statistics and Probability.* Berkeley: Univ. Calif. Press, 1967, vol. 1, pp. 281–297.

Peter Kruizinga received the M.S. degree in computer science from the University of Groningen, The Netherlands, in 1993. Since 1993, he has been pursuing the Ph.D. degree at the Department of Computing Science, University of Groningen.

His main interests are texture analysis and computer models of visual neurons for texture processing.
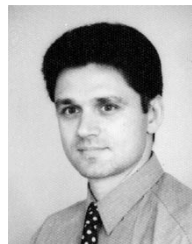
Nikolay Petkov received the M.S. degree in physics from the University of Sofia, Bulgaria, in 1980, and the Dr.sc.techn. degree in computer engineering from Dresden University of Technology, Germany, in 1987.

Currently, he holds a chair of Parallel Computing at the University of Groningen, The Netherlands. He is the author of two books and more than 60 scientific publications. His current research interests are in the area of computer simulations of the visual system.